A fast boundary-finite element approach for estimating anchor losses in Micro-Electro-Mechanical System resonators

A fast boundary-finite element approach for estimating anchor losses in Micro-Electro-Mechanical System resonators

A. Aimi[a], L. Desiderio[a,*], P. Fedeli[b], A. Frangi[c]

[a] *Department of Mathematical, Physical and Computer Sciences, University of Parma*
Parco Area delle Scienze, 53/A, 43124, Parma, Italy
[b] *AMS R&D STMicroelectronics, Geneve, Switzerland*
[c] *DICA, Politecnico di Milano, Piazza Leonardo da Vinci, 32, 20133, Milano, Italy*

Abstract

This paper is focused on a fast and reliable estimate of anchor energy losses from a Micro-Electro-Mechanical System resonator, working at pressure in the order of the microbar, due to the scattering of elastic waves from the resonator into the substrate to which it is attached. The proposed numerical method is based on the fundamentals of the analytical procedure employed to estimate quality factors of resonators in the literature and consists in the modeling of the resonator by Finite Elements and of the radiated waves dissipation into the substrate by collocation Boundary Element Method. In order to simulate as quickly as possible an accurate response of the substrate in real time, we further consider $\mathcal{H}$-matrix/vector product in the Boundary Element Method. The proposed numerical approach results in a very small elapsed computational time and it will therefore allow applications to real life engineering problems, targeted as future investigations.

Keywords: frequency-domain Boundary Element Method, Finite Element Method, Micro-Electro-Mechanical System resonator, anchor losses, wave dissipation, $\mathcal{H}$-matrix

1. Introduction

Micro-Electro-Mechanical System (MEMS) resonators are relatively new but surging component of modern electronics and communication technologies in areas such as timing, navigation, RF & wireless communications, gaming and personal electronics (see [1] and references therein). In a MEMS resonator, its micromechanical structure is fixed on a substrate, much larger w.r.t. the former. The resonator is periodically excited to one of its natural resonance modes at a single frequency and a voltage signal is generated from its response periodic vibrations, during which the structure exerts a time-harmonic stress on the foundation through its clamped region. Acting as an excitation source, this time-harmonic stress results in an energy loss, commonly referred to as anchor loss, due to waves traveling from the resonator to the substrate. The rate of the energy dissipation is described by a quality factor Q, that standardizes the performances of the resonator and is defined as the ratio between the maximum stored energy W and the energy lost per cycle ΔW, i.e.

$$Q := 2\pi \frac{W}{\Delta W}. \tag{1}$$

An accurate estimate of Q is of fundamental importance, since it directly translates into information about the performances of the resonator products, such as high sensitivities, better bias stability, and improved frequency selectivity. Unfortunately, the evaluation of the anchor loss is a very delicate point, since it involves not only the device (typically a volume less than 1 mm^3), but also the substrate. For this reason, a separation and transfer method has been developed [2] that

*Corresponding author
Email addresses: alessandra.aimi@unipr.it (A. Aimi), luca.desiderio@unipr.it (L. Desiderio), patrick.fedeli@polimi.it (P. Fedeli), attilio.frangi@polimi.it (A. Frangi)

decouples the MEMS structure and the substrate. Taking into account the negligible interference between the vibrations in the device and the elastic wave propagation in the foundation, the classic vibration theory is used to describe the elastic vibrations in the resonator with the anchor clamped but suffering from a time-harmonic stress. In many applications, a closed-form expression for this stress at the clamped region is known, as well as the maximum vibration energy Q stored in the device. If one assumes that all the vibration energy entering the substrate is lost, i.e. it does not return to the resonator, the foundation can be conceived as a semi-infinite medium, where the time-harmonic displacement at the junction, corresponding to the stress from the vibrations of the resonator, has to be computed in order to calculate ΔW.

Various methodologies have been addressed for providing analytical estimates of the energy loss, even if they are based on simplifying assumptions which are generally difficult to quantify. In [3], the energy loss from a cantilever resonator into a semi-infinite elastic medium is considered and it is analytically quantified by comparing the vibration energy of the cantilever with the elastic energy generated in the elastic medium by the shear force and bending moment acting at the root of the cantilever. In [4], the authors provide an estimate of the energy loss associated to the elastic wave transmission across the junction between two plates of differing widths but same thickness. The case of a 3D cantilever beam attached either to a semi-infinite space or to a semi-infinite plate of finite thickness is analytically investigated in [5]. All these techniques have been generalized by using the framework of radiation tunneling in photonics [6, 7]. In conclusion, even if some analytical estimates based on physical model simplifications have been given, the need of a robust, fast and accurate numerical method is highly desirable.

From this perspective, even though some numerical techniques have been developed for the simulation of the dissipation due to thermoelastic damping [8, 9], the issue of anchor losses is still almost uninvestigated from the numerical point of view. The difficulty in the design of an efficient and accurate numerical strategy lies in the fact that the substrate is virtually a semi-infinite medium and, consequently, cannot be simulated with Finite Difference (FD) or Finite Element (FE) analysis softwares. To overcome this drawback, one can draw from the large body of the literature on the investigation of wave propagation in semi-infinite or infinite media, enriched by authors who proposed numerical schemes based on the Boundary Element Method (BEM) in both time (see e.g. [10, 11, 12]) and frequency-domain (see e.g. [13, 14, 15, 16, 17]), and on the coupling between BEM and FEM (see e.g. [18, 19]).

Hence, in this work, following the fundamentals of some of the above recalled analytical procedures, we develop an efficient approach, treating the microstructure with Finite Elements and the unbounded substrate with Boundary Elements. In fact, it is well known that for problems involving subregions with different geometrical properties, a natural approach is to combine FEM and BEM within a unified computational model, thus making use of the advantages that both methods offer. Further, the introduction of $\mathcal{H}$-matrix/vector product in the BEM allows to speed up the computation in the substrate and to give real-time and accurate numerical responses.

Let us note that a similar approach, where only a suitable one-shot coupling between FEM and BEM is needed, was introduced and analyzed in [1] for 2D model problems, but not deeply numerically investigated for 3D benchmarks, and using Perfectly Matched Layers (PMLs) instead of BEM.

Let us finally remark that, treating microstructure and foundation as a unified BEM domain would give rise to a nonlinear eigenvalue problem, whose solution can be obtained by means of several approximations and with a sensibly heavy computational cost (see e.g. [20, 21]).

The paper is structured as follows: in the following Section we introduce the background differential model problem and its governing equations, then we describe the numerical FEM and BEM modeling and the algorithm for quality factor evaluation in Section 3, while several numerical results related to both axial and bending modes are shown and discussed in Section 4. A conclusive Section ends the paper.

2. Background model problem and its governing equations

In a fixed Cartesian coordinates system $\mathbf{x} = (x_1, x_2, x_3)^\top$, the frequency-domain elastic wave equation for a homogeneous medium $\Omega \subset \mathbf{R}^3$ (for simplicity we postulate the absence of body forces) is given by

$$\frac{E}{2(1+\nu)}\boldsymbol{\Delta}\mathbf{u}(\mathbf{x}) + \frac{E}{2(1+\nu)(1-2\nu)}\boldsymbol{\nabla}\boldsymbol{\nabla}\cdot\mathbf{u}(\mathbf{x}) + \varrho\omega^2\mathbf{u}(\mathbf{x}) = \mathbf{0}, \tag{2}$$

where E is the Young's modulus, ν is the Poisson's ratio, ϱ is the mass density and ω is the circular frequency. The unknown vector $\mathbf{u}(\mathbf{x})$ stands for the displacement field. Furthermore, $\boldsymbol{\Delta}$ and $\boldsymbol{\nabla}$ denote the Laplace and the Nabla operators, respectively.
Eq. (2) can be obtained from the combination of the following basic mechanical equations [22]:

$$\boldsymbol{\nabla}\cdot\boldsymbol{\sigma}[\mathbf{u}](\mathbf{x}) + \varrho\omega^2\mathbf{u}(\mathbf{x}) = \mathbf{0} \tag{3a}$$
$$\boldsymbol{\sigma}[\mathbf{u}](\mathbf{x}) = \mathbf{C} : \boldsymbol{\varepsilon}[\mathbf{u}](\mathbf{x}) \tag{3b}$$
$$\boldsymbol{\varepsilon}[\mathbf{u}](\mathbf{x}) = \frac{1}{2}\left[\boldsymbol{\nabla}\mathbf{u}(\mathbf{x}) + \boldsymbol{\nabla}\mathbf{u}(\mathbf{x})^\top\right], \tag{3c}$$

where $\boldsymbol{\sigma}[\mathbf{u}](\mathbf{x})$ and $\boldsymbol{\varepsilon}[\mathbf{u}](\mathbf{x})$ are, respectively, the second order stress and strain tensors, while $\mathbf{C}$ is the fourth order stiffness tensor. In Eq. (3b) and in the following, the symbol ":" denotes the double tensor inner product. Eq. (3a) is the momentum equilibrium equation; Eq. (3b) represents the constitutive law of the linear elastic model and Eq. (3c) stands for kinematical relations.
If the boundary $\partial\Omega$ of the problem domain is decomposed as $\partial\Omega = \Gamma_{\text{D}} \cup \Gamma_{\text{N}}$ with $\Gamma_{\text{D}} \cap \Gamma_{\text{N}} = \emptyset$ (Γ_{D} stands for the Dirichlet boundary and Γ_{N} stands for the Neumann boundary), the boundary conditions of the elastodynamic problem are given by

$$\mathbf{u}(\mathbf{x}) = \bar{\mathbf{u}}(\mathbf{x}) \qquad \text{on } \Gamma_{\text{D}} \tag{4a}$$
$$\mathbf{t}(\mathbf{x}) = \boldsymbol{\sigma}[\mathbf{u}](\mathbf{x})\cdot\mathbf{n}(\mathbf{x}) = \bar{\mathbf{t}}(\mathbf{x}) \qquad \text{on } \Gamma_{\text{N}}, \tag{4b}$$

where the prescribed values are indicated by over bars and $\mathbf{t}(\mathbf{x})$ is the traction vector along the boundary, whose unit outward normal vector in $\mathbf{x}$ is represented by $\mathbf{n}(\mathbf{x})$.

In the present work, Ω denotes a resonating MEMS attached to a much larger substrate. We decompose Ω into a bounded subdomain Ω_{F}, occupied by the resonator and by a hemispherical portion of the foundation, and into its complement Ω_{B}, which allows the elastic waves radiation and dissipation, as depicted in a 2D section perspective in Figure 1. The FEM will be used to discretize the problem in Ω_{F}, while the BEM will be employed for the subdomain Ω_{B}. The two subdomains are supposed to be non-overlapping and the portion of the boundary shared by Ω_{F} and Ω_{B} is the interface $\Gamma_{\text{I}} = \partial\Omega_{\text{F}} \cap \partial\Omega_{\text{B}}$. From now on, $\Gamma_{\text{F}} = \partial\Omega_{\text{F}} \setminus \Gamma_{\text{I}}$ and $\Gamma_{\text{B}} = \partial\Omega_{\text{B}} \setminus \Gamma_{\text{I}}$ are both supposed traction free, i.e. $\bar{\mathbf{t}} = \mathbf{0}$.
In a classical BEM-FEM coupling, continuity of the displacement field and equilibrium of the traction field across Γ_{I} are usually enforced through the following strong transmission conditions:

$$\mathbf{u}_{\text{F}}(\mathbf{x}) = \mathbf{u}_{\text{B}}(\mathbf{x}) \qquad \text{on } \Gamma_{\text{I}} \tag{5a}$$
$$\mathbf{t}_{\text{F}}(\mathbf{x}) = -\mathbf{t}_{\text{B}}(\mathbf{x}) \qquad \text{on } \Gamma_{\text{I}}, \tag{5b}$$

where the subscripts F and B indicate if a variable is related to the FEM or the BEM subdomain, respectively. In the following we will use only (5b). In fact, since the FEM subdomain produces forces related to the vibration mode of the resonator, the focus here is to apply these forces on the BEM subdomain to estimate radiation loss. This approach is similar to the analytical one, but avoids simplified formulas and can be applied to every type of structure.

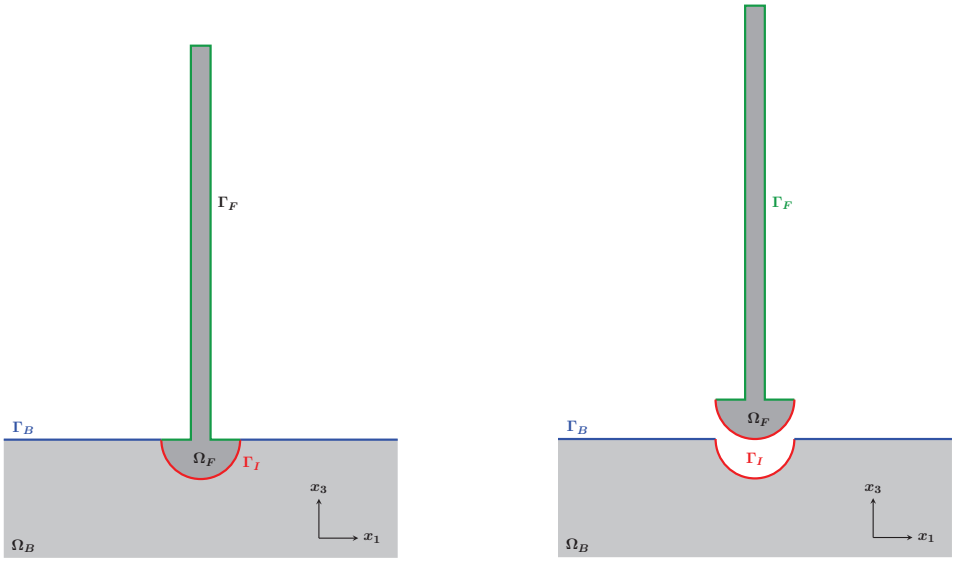

Figura 1: Spatial domain decomposition: original problem defined in the semi-infinite domain Ω (resonating MEMS attached to a larger substrate) on the left; decomposition in the two non-overlapping subdomains Ω_{F} (discretized by FEM) and Ω_{B} (discretized by BEM) on the right. The portion of surface shared by the two subdomains is the interface Γ_{I}.

3. The proposed numerical approach

3.1. Finite Element Modelling

In the FEM subdomain Ω_{F}, the interface Γ_{I} is considered as an essential boundary, i.e. the displacement $\bar{\mathbf{u}}(\mathbf{x})$ is imposed on Γ_{I}. The integral weak-form of the governing Eq. (3a) can be written as:

$$-\omega^2 \int_{\Omega_{\mathrm{F}}} \varrho \mathbf{u}(\mathbf{x}) \cdot \mathbf{v}(\mathbf{x}) \, \mathrm{d}\mathbf{x} + \int_{\Omega_{\mathrm{F}}} \boldsymbol{\sigma}[\mathbf{u}](\mathbf{x}) : \boldsymbol{\varepsilon}[\mathbf{v}](\mathbf{x}) \, \mathrm{d}\mathbf{x} = 0 \,, \tag{6}$$

where $\mathbf{v}(\mathbf{x})$ stands for a virtual displacement (weight function), which is assumed in the Sobolev space $\mathbf{H}^1_{\Gamma_{\mathrm{I}}}(\Omega_{\mathrm{F}}) := \left\{ \mathbf{v} \in \left[\mathrm{H}^1(\Omega_{\mathrm{F}})\right]^3 \mid \mathbf{v}(\mathbf{x}) = \mathbf{0} \text{ on } \Gamma_{\mathrm{I}} \right\}$. Taking into account Eq. (3b), the final form of Eq. (6) becomes

$$\int_{\Omega_{\mathrm{F}}} \boldsymbol{\varepsilon}[\mathbf{u}](\mathbf{x}) : \mathbf{C} : \boldsymbol{\varepsilon}[\mathbf{v}](\mathbf{x}) \, \mathrm{d}\mathbf{x} = \omega^2 \int_{\Omega_{\mathrm{F}}} \varrho \mathbf{u}(\mathbf{x}) \cdot \mathbf{v}(\mathbf{x}) \, \mathrm{d}\mathbf{x} \,. \tag{7}$$

At this level, we employ a standard Galerkin finite element discretization. In this work, we choose a partitioning of the domain Ω_{F} into ten nodes tetrahedral finite elements. On this tessellation, a set of basis functions is defined and used to interpolate each component of the solution and of the boundary datum. The nodes of the mesh are chosen as interpolation points. Standard FEM requires basis function from the Sobolev space $H^1(\Omega_{\mathrm{F}})$ [23]. According to the choice of finite elements, we use standard piecewise quadratic polynomial basis functions, which are C^0-continuous across elements. By adopting these basis functions as weight functions, equation (7) is discretized by

$$\mathbb{K}\,\mathbf{u}_{\mathrm{F}} = \omega^2 \mathbb{M}\,\mathbf{u}_{\mathrm{F}}, \tag{8}$$

where $\mathbb{M}$ and $\mathbb{K}$ stand, respectively, for positive definite mass matrix and semi-positive definite stiffness matrix, both real and symmetric, of the model, and the vector $\mathbf{u}_{\mathrm{F}}$ collects the nodal displacement, both known and unknown, in $\Omega_{\mathrm{F}} \cup \partial\Omega_{\mathrm{F}}$.

Let us note that the FEM matrices $\mathbb{M}$ and $\mathbb{K}$ are generated with linear computational cost and require linear memory storage, i.e. $O(N_{\mathrm{F}})$ with N_{F} being the total number of degrees of freedom in the FEM subdomain.

At first, we consider, excited in its axial/bending modes, a perfectly clamped isolated MEMS, i.e. we impose $\bar{\mathbf{u}}(\mathbf{x}) = \mathbf{0}$ on Γ_{I} and, remembering the already cited boundary condition $\bar{\mathbf{t}}(\mathbf{x}) = \mathbf{0}$ on Γ_{F}, the generalized eigenvalue problem (8) is solved, by means of an iterative algorithm based on Implicitly Restarted Arnoldi Method (IRAM) [24].
Then, taking into account the eigenvalue $\widetilde{\omega}$ of interest and related eigenvector $\tilde{\mathbf{u}}_{\text{F}}$, in a post-processing phase the corresponding traction $\tilde{\mathbf{t}}^{\text{I}}_{\text{F}}$ on the interface Γ_{I} is evaluated and successively used as Neumann boundary datum in the BEM subdomain.

Remark 1. Note that $\widetilde{\omega}$ can be considered as an approximation of the real part of the eigenfrequency of Eq. (2), conceived as a generalized eigenvalue problem on the whole domain Ω. The choice of quadratic, instead of classical linear, finite element shape functions will allow to recover an accurate value of $\widetilde{\omega}$, which is a key point for the successive computation in BEM subdomain.

3.2. Boundary Element Modelling

In the BEM subdomain Ω_{B}, the interface Γ_{I} is considered as a natural boundary, i.e. the traction $\mathbf{t}(\mathbf{x}) = \bar{\mathbf{t}}(\mathbf{x})$ is imposed on Γ_{I}. For any point $\mathbf{x} \in \Omega_{\text{B}} \setminus \partial\Omega_{\text{B}}$, the Somigliana integral representation formula of the unknown displacement field has the form

$$\mathbf{u}(\mathbf{x}) = \int_{\partial\Omega_{\text{B}}} \mathbf{U}_{\omega}(\mathbf{x},\mathbf{y})\,\mathbf{t}(\mathbf{y})\;\mathrm{d}\Gamma_{\mathbf{y}} - \int_{\partial\Omega_{\text{B}}} \mathbf{T}_{\omega}(\mathbf{x},\mathbf{y})\,\mathbf{u}(\mathbf{y})\;\mathrm{d}\Gamma_{\mathbf{y}}, \tag{9}$$

where $\mathbf{U}_{\omega}(\mathbf{x},\mathbf{y})$ and $\mathbf{T}_{\omega}(\mathbf{x},\mathbf{y})$ represent the second order fundamental displacement and traction tensors, respectively. Since we have only Neumann boundary conditions on $\partial\Omega_{\text{B}}$, and in particular $\mathbf{t}(\mathbf{x}) = \mathbf{0}$ on Γ_{B}, Eq.(9) becomes:

$$\mathbf{u}(\mathbf{x}) = \int_{\Gamma_{\text{I}}} \mathbf{U}_{\omega}(\mathbf{x},\mathbf{y})\,\bar{\mathbf{t}}(\mathbf{y})\;\mathrm{d}\Gamma_{\mathbf{y}} - \int_{\partial\Omega_{\text{B}}} \mathbf{T}_{\omega}(\mathbf{x},\mathbf{y})\,\mathbf{u}(\mathbf{y})\;\mathrm{d}\Gamma_{\mathbf{y}}. \tag{10}$$

Allowing $\mathbf{x} \in \Omega_{\text{B}}$ to approach the boundary with the help of a limiting process [25], since a singularity occurs in $\mathbf{y} = \mathbf{x}$ when $\mathbf{x} \in \partial\Omega_{\text{B}}$, the frequency-domain Boundary Integral Equation for the elastodynamic problem for smooth surfaces can be written in the form:

$$\frac{1}{2}\mathbf{u}(\mathbf{x}) = \int_{\Gamma_{\text{I}}} \mathbf{U}_{\omega}(\mathbf{x},\mathbf{y})\,\bar{\mathbf{t}}(\mathbf{y})\;\mathrm{d}\Gamma_{\mathbf{y}} - (\text{C.P.V.}) \int_{\partial\Omega_{\text{B}}} \mathbf{T}_{\omega}(\mathbf{x},\mathbf{y})\,\mathbf{u}(\mathbf{y})\;\mathrm{d}\Gamma_{\mathbf{y}}\,, \tag{11}$$

where the second surface integral in the right-hand side has to be understood as Cauchy Principal Value.
The discretization of Eq. (11), where $\omega = \widetilde{\omega}$ is kept fixed, begins with a fine approximation of $\partial\Omega_{\text{B}}$ using a system of three nodes triangular surface elements. Let us note that on Γ_{I} the BEM and FEM meshes have to coincide. The unknown displacement and the known traction fields over each element are interpolated independently through shape functions. The functional background compels one to choose shape functions belonging to $\mathbf{L}^2(\partial\Omega_{\text{B}})$ for the approximation of $\mathbf{t}(\mathbf{x})$ and to $\mathbf{H}^1(\partial\Omega_{\text{B}})$ for the approximation of $\mathbf{u}(\mathbf{x})$. In the following, we consider linear interpolation shape functions for the components of the displacement and constant shape functions for the components of the traction. Finally, the surface mesh nodes are also used as collocation nodes. In this way, we obtain the following linear system of equations

$$\left(\frac{1}{2}\mathbb{I} + \mathbb{D}\right)\,\mathbf{u}_{\text{B}} = \mathbb{V}\,\bar{\mathbf{t}}_{\text{B}}, \tag{12}$$

where $\mathbb{I}$ stands for the identity matrix, while $\mathbb{D}$ and $\mathbb{V}$ are complex influence matrices. In the following, we denote by $\mathbb{H}$ the matrix of the BEM system, i.e. $\mathbb{H} = \frac{1}{2}\mathbb{I} + \mathbb{D}$. In Eq. (12), $\mathbf{u}_{\text{B}}$ and $\bar{\mathbf{t}}_{\text{B}}$ stand for the unknown nodal displacement and the known traction vectors, respectively.

Separating the degrees of freedom on Γ_{B} from those on Γ_{I}, such that $\mathbf{u}_{\text{B}} = [\mathbf{u}_{\text{B}}^{\text{B}} \;\; \mathbf{u}_{\text{B}}^{\text{I}}]^{\top}$ and $\bar{\mathbf{t}}_{\text{B}} = [\mathbf{0} \;\; \mathbf{t}_{\text{B}}^{\text{I}}]^{\top}$, yields:

$$\begin{bmatrix} \mathbb{H}_{\text{BB}} & \mathbb{H}_{\text{BI}} \\ \mathbb{H}_{\text{IB}} & \mathbb{H}_{\text{II}} \end{bmatrix} \begin{bmatrix} \mathbf{u}_{\text{B}}^{\text{B}} \\ \mathbf{u}_{\text{B}}^{\text{I}} \end{bmatrix} = \begin{bmatrix} \mathbb{V}_{\text{BB}} & \mathbb{V}_{\text{BI}} \\ \mathbb{V}_{\text{IB}} & \mathbb{V}_{\text{II}} \end{bmatrix} \begin{bmatrix} \mathbf{0} \\ \mathbf{t}_{\text{B}}^{\text{I}} \end{bmatrix}. \tag{13}$$

In general, the square matrix $\mathbb{H}$ is non-symmetric (due to the collocation approach) and fully-populated, with $O(N_{\text{B}}^2)$ memory requirement, where N_{B} is the total number of degrees of freedom in the BEM subdomain. However, looking at Eq. (11), we note that the computation of the entries of matrix $\mathbb{H}$ requires the evaluation of the tensor $\mathbf{T}_{\omega}(\mathbf{x}, \mathbf{y})$ on $\partial\Omega_{\text{B}}$. In [13], it has been shown that, as soon as $\mathbf{x}$ and $\mathbf{y}$ belong to the same plane (let's say $x_3 = y_3 = 0$ for simplicity), this Green's tensor simplifies as

$$\mathbf{T}_{\omega}(\mathbf{x}, \mathbf{y}) = \begin{bmatrix} 0 & 0 & a\, r_{,1} \\ 0 & 0 & a\, r_{,2} \\ a\, r_{,1} & a\, r_{,2} & 0 \end{bmatrix}, \tag{14}$$

where the constant a depends only on E, ν, ϱ, ω and $r_{,i}$ is the derivative of $r := \|\mathbf{x} - \mathbf{y}\|_2$ with respect to y_i. Since in our application Γ_{B} is a large planar surface, the number of entries that we have to compute in order to assemble the matrix $\mathbb{H}$, composed by sub-blocks of the same type as in the right-hand side of (14), is less than $N_{\text{B}}^2/2$. The storage, performed in sparse column format, give some memory saving too, as we will in Section 4. Additionally, the matrix-vector product can be performed with half computational cost w.r.t. purely quadratic one, by taking into account the position of the non-zero entries of $\mathbb{H}$. This is an essential task when an iterative method, typically GMRES [26], is used to solve system (13).

Unfortunately, the rectangular matrix $\mathbb{V}$ does not have the same structure of $\mathbb{H}$ and it is dense, but the RHS of Eq. (13) can be computed by replacing $\mathbb{V}$ with its $\mathcal{H}$-matrix representation $\mathbb{V}_{\mathcal{H}}$ and by taking advantage of the fast $\mathcal{H}$-matrix/vector product, with logarithmic linear complexity instead of quadratic complexity of the standard matrix/vector product [27].
The construction of the $\mathcal{H}$-matrix representations of $\mathbb{V}$ requires a hierarchical subdivision of $\mathbb{V}$ based on geometrical considerations. First, a hierarchical cluster tree $T_{\mathcal{I}}$ is constructed based on the boundary element mesh. At level 0, the cluster consists of the complete mesh. Each cluster is recursively partitioned into two sons, until the clusters contain at most a prescribed number n_{LEAF} of elements. Each cluster-pair (X, Y) defines a sub-block of the matrix, that is imposed to the following admissibility condition:

$$\max\{\text{diam } X, \text{diam } Y\} \leq \eta\, \text{dist}(X, Y), \tag{15}$$

where diam X (resp. diam Y) is the diameter of a block domain X (resp. Y), $\text{dist}(X, Y) = \inf\{\|\mathbf{x} - \mathbf{y}\|_2,\ \mathbf{x} \in X,\ \mathbf{y} \in Y\}$ is the Euclidean distance between the domains X and Y and $\eta > 0$ is the admissibility parameter of the method. Sub-blocks satisfying (15) are marked as admissible, otherwise they are called non-admissible. The former are low-rank matrices and they are stored in so-called outer-product form with a drastic reduction of their memory requirement; the latter are full-rank matrices and they have to be stored as dense matrices with a cost of the order of $\mathcal{O}(n_{\text{LEAF}}^2)$.
The crucial point for computing the $\mathcal{H}$-matrix representation $\mathbb{V}_{\mathcal{H}}$ is an accurate and rank revealing algorithm to perform low-rank approximations of the admissible blocks. In the case of 3D elastodynamics, a good strategy is the vectorial generalization of the partially-pivoted Adaptive Cross Approximation (ACA) [28], which firstly appeared in [29], was found independently in [13] and recently used in the elasticity framework [14, 30]. This algorithm computes adaptively the rank required to guarantee a prescribed accuracy $\varepsilon_{\text{ACA}} > 0$, that represents a good measure not only of the error on the approximation of the whole BEM matrix, but also of the accuracy of the $\mathcal{H}$-matrix/vector product, although computed in Frobenius norm [13]. Further, it has been shown

in [13] that even though the $\mathcal{H}$-matrix construction is not optimal in the case of Helmholtz and oscillatory elastodynamic kernels, substantial memory savings are achieved in practice.
The $\mathcal{H}$-matrix representation of $\mathbb{V}$ allows us to accelerate the computation of the RHS of Eq. (13). The accelerated matrix/vector product is performed hierarchically by going through the $\mathcal{H}$-matrix representation. At the leaf level, there are two possibilities. If the block is marked as non-admissible, the standard matrix-vector product is used. Otherwise, if the block is marked as admissible, its low-rank approximation is used to reduce the cost of the standard matrix/vector product.
It is known [31] that the storage requirement for the matrix $\mathbb{V}_{\mathcal{H}}$ is $O(N_{\mathrm{B}} \log(N_{\mathrm{B}}))$. We mention here that an efficient implementation based on an on-the-fly multiplication of the dense matrix $\mathbb{V}$ with the vector $\bar{\mathbf{t}}_{\mathrm{B}}$ gives a linear storage of $\mathbb{V}\bar{\mathbf{t}}_{\mathrm{B}}$, but implies a full quadratic computational cost. Hence, our approach turns to be faster as much less entries are computed.

To conclude, considering that matrix $\mathbb{H}$ is not represented as a hierarchical matrix but has a large number of zero entries, even if the overall algorithm has still quadratic complexity, the amount of memory and computational resources required to solve the system iteratively is by a factor of 60% smaller. Further, the evaluation of the RHS using the $\mathcal{H}$-matrix representation of $\mathbb{V}$ helps in reducing the elapsed time of the BEM computation, as it will be specified in the next subsection.

Remark 2. The choice of collocation BEM instead of a Galerkin BEM approach has been made to avoid a double integration process in the construction of the entries of matrices $\mathbb{D}$ and $\mathbb{V}$, in order to reduce as much as possible the computational time of the BEM part of the one-shot coupling with FEM. The drawback is the lack of a complete convergence theory as one can find in the Galerkin setting. Anyway, based on numerical evidence, the relation between the order of the meshsizes and the order of accuracy on Q will be highlighted in the sequel.

3.3. Quality factor evaluation

The numerical approach here proposed mimics the fundamentals of the analytical procedure employed to estimate quality factors of resonators in the literature [3, 5, 32], but the influence of the additional hemisphere makes the proposed approach more reliable than the analytical one. As already described above, at first the clamped isolated MEMS is analysed imposing homogeneous Dirichlet datum on Γ_{I}. The eigenvalue problem (8) is solved using FEM, in order to compute the frequency $\widetilde{\omega}$ corresponding to the desired mode. Then, the value of the maximum elastic energy stored in the MEMS is estimated as

$$W = \frac{1}{2}\,\widetilde{\omega}^2 \tag{16}$$

and the evaluated parameter $\widetilde{\omega}$ is then considered fixed for the computation in the substrate, i.e. in the BEM subdomain. Further, the corresponding traction $\tilde{\mathbf{t}}^{\mathrm{I}}_{\mathrm{F}}$ is successively computed as projection of the stress state.
Then, remembering (5b), $\mathbf{t}^{\mathrm{I}}_{\mathrm{B}} = -\tilde{\mathbf{t}}^{\mathrm{I}}_{\mathrm{F}}$ is imposed as Neumann boundary condition on Γ_{I} for the BEM problem in the substrate alone and $\mathbf{u}^{\mathrm{I}}_{\mathrm{B}}$ is computed by solving Eq. (12). To estimate the quality factor (1), we use the values of the computed displacement $\mathbf{u}^{\mathrm{I}}_{\mathrm{B}}$ and traction $\mathbf{t}^{\mathrm{I}}_{\mathrm{B}}$ in order to approximate the dissipation of energy ΔW in the substrate Ω_{B}, defined as (see [1], page 259):

$$\Delta W := \pi \int_{\Gamma_{\mathrm{I}}} \Im[\mathbf{u}(\mathbf{x}) \cdot \mathbf{t}(\mathbf{x})] d\Gamma_{\mathbf{x}}\,. \tag{17}$$

We remark that, because of the choice of linear interpolation shape functions for the components of $\mathbf{u}^{\mathrm{I}}_{\mathrm{B}}$ and constant shape functions for the components of $\mathbf{t}^{\mathrm{I}}_{\mathrm{B}}$, the dissipation of energy can be nicely approximated in the following way:

$$\Delta W \simeq \frac{\pi}{3} \sum_{k=1}^{N_{\Gamma_{\mathrm{I}}}} |\mathrm{E}_k|\, \Im\left(\mathbf{t}^{\mathrm{I}}_{\mathrm{B},\mathrm{E}_k} \cdot \widetilde{\mathbb{I}} \cdot \mathbf{u}^{\mathrm{I}}_{\mathrm{B},\mathrm{E}_k}\right), \tag{18}$$

where $\{\mathrm{E}_k,\ k = 1, \ldots, N_{\Gamma_\mathrm{I}}\}$ represents the set of triangular surface elements approximating the interface Γ_I, $|\mathrm{E}_k|$ denotes the measure of the element E_k, the vector $\mathbf{u}^\mathrm{I}_{\mathrm{B},\mathrm{E}_k}$ collects the values of the three components of the displacement field at the vertices of the triangle E_k, while the vector $\mathbf{t}^\mathrm{I}_{\mathrm{B},\mathrm{E}_k}$ contains the three components of the traction at the mass center of E_k. Furthermore, in (18) $\widetilde{\mathbb{I}}$ stands for the matrix obtained by putting three identity matrices of order 3 side by side.

The above procedure is summarized in the following algorithm:

One-shot BEM-FEM approach for estimating anchor losses in MEMS resonators

1. Mesh the domain Ω_F (meshsize h_F) and consider quadratic shape functions for displacement field
2. Mesh the surface $\partial\Omega_\mathrm{B}$ (meshsize $h_\mathrm{B} \simeq h_\mathrm{F}$) and consider linear and constant shape functions respectively for displacement and traction fields
3. Compute the frequency $\widetilde{\omega}$ corresponding to the desired mode, solving the eigenvalue-eigenvector discrete problem (8) using IRAM, in the FEM subdomain
4. Deduce the maximum elastic energy W stored in the MEMS with formula (16)
5. Compute the traction $\tilde{\mathbf{t}}^\mathrm{I}_\mathrm{F}$ on Γ_I in the FEM subdomain
6. Impose $\mathbf{t}^\mathrm{I}_\mathrm{B} = -\tilde{\mathbf{t}}^\mathrm{I}_\mathrm{F}$ as Neumann boundary condition on Γ_I for the BEM problem
7. Compute the displacement $\mathbf{u}^\mathrm{I}_\mathrm{B}$ solving the linear system (12) using GMRES, in the BEM subdomain
8. Approximate the energy dissipation ΔW using formula (18) with the computed $\mathbf{u}^\mathrm{I}_\mathrm{B}$ and $\mathbf{t}^\mathrm{I}_\mathrm{B}$
9. Evaluate quality factor Q using (1)

Note that the leading computational cost in the FEM subdomain, due to the use of IRAM iterative algorithm for the numerical approximation of eigenvalues and eigenvectors, will be $O(N_\mathrm{F})$ per iteration. On the other side, the principal computational cost in the BEM subdomain is the numerical solution of (12) by GMRES, which involves $\frac{N_\mathrm{GMRES}}{2} O(N_\mathrm{B}^2) + N_\mathrm{B} \log(N_\mathrm{B})$ operations, where N_GMRES is the number of iterations, choosing the $\mathcal{H}$-matrix representation of $\mathbb{V}$. The computational cost saving percentage in using this representation is $\frac{N_\mathrm{B} - \log(N_\mathrm{B})}{(\frac{N_\mathrm{GMRES}}{2}+1)O(N_\mathrm{B})}$: the less the iterations until convergence, the higher the elapsed time saving.
Numerical results, reported in the next Section, show an $O(h_\mathrm{B})$ accuracy in the approximation of Q, as long as a careful numerical evaluation of the eigenfrequency $\widetilde{\omega}$ has been done. For this reason, in the above algorithm we suggest to consider, having fixed $h_\mathrm{F} \simeq h_\mathrm{B}$, higher degree shape functions in the FEM than in the BEM subdomain.
Finally, it's worth noting that, in the performed simulations, for fixed meshsizes of order $O(10^{-1})$ the algorithm has furnished reliable estimates of the quality factor until an $O(10^6)$ order of magnitude, but in this last scenario, huge quality factors have little engineering significance, since in this case dissipative phenomena other than anchor losses usually dominate.

4. Numerical results

In this section, we focus on the 3D benchmark of a cantilever beam resting on a semi-infinite space. A similar benchmark can be found in [1], but here we have considered a rectangular transversal section, instead of squared, to generalize the geometry of the resonator. The simple configuration allowed us to compare numerical results with analytical estimates findable in literature, but differently from the latter the proposed approach can be applied to every type of structure.
The algorithm involves separate computations of the FEM and BEM local problems defined respectively on Ω_F and $\partial\Omega_\mathrm{B}$. The FEM formulation has been implemented in a Fortran code, developed at Politecnico of Milano, Italy. The Arpack [33] library coupled with the direct linear solver Pardiso [34], has been employed for the extraction of eigenvalues and eigenvectors. This

software has been used in black-box fashion. The BEM formulation has been implemented in a prototype `Matlab` code, on the basis of the Fortran code in [35] and employing `Matlab` built-in function `GMRES` for the solution of the BEM system, modified in order to take into account the position of the non-zero entries of the matrix $\mathbb{H}$. We have also implemented a `Matlab` software library for hierarchical matrices, that offers data structures for clusters, blocks, low-rank matrices and $\mathcal{H}$-matrices, an algebraic compression scheme for non-local operators, based on the vectorial form of the standard ACA, and an efficient algorithm for $\mathcal{H}$-matrix/vector product.

4.1. Definition of the test problems

We fix the length of the resonator $L = 10\,\mu$m, its height $H = 0.5\,\mu$m and its width $V = 1\,\mu$m. The interface between the MEMS and the substrate is the hemispherical surface of radius $R_1 = 1\,\mu$m. Further, we consider a truncated version of the foundation, bounded by the circle of radius $R_2 = 5\,\mu$m. Enlargements of the considered portion of the substrate have been taken into account, without giving significant improvement of the results. This happens because the recovered displacements rapidly decay away from the resonator anchor, so that contributions of the neglected part of the boundary $\partial\Omega_{\text{B}}$ are vanishing. Hence, the choice of an external radius quintuple of the internal one revealed a good choice in order to avoid spurious reflections, as it will be clear looking at recovered displacements fields, allowing a smooth dissipation of the waves.
Both the cantilever and the substrate are made of silicon, with mass density $\varrho = 2,300\,\text{kg/m}^3$ and Young's modulus $E = 160,000\,\text{MPa}$. We choose the Poisson's ratio $\nu = 0.33$.
The surface $\partial\Omega_{\text{B}}$ is discretized with $14,342$ three nodes triangular elements with size $h_{\text{B}} \leq 0.2141\,\mu$m and $7,298$ collocation nodes, while the FEM volume Ω_{F} is meshed with $9,332$ ten nodes isoparametric quadratic tetrahedral elements with size $h_{\text{F}} \leq 0.125\,\mu$m and $37,693$ nodes: the choice of such fine meshes will ensure good approximation properties, with discretization errors of the overall procedure behaving at least linearly with the meshsize, and is allowed by the fast approach here taken into account. Since non-matching FEM and BEM nodes are considered, tractions computed at the FEM nodes have to be linked to their respective values at the BEM nodes. In particular, we choose a linear interpolation scheme, where a variable on Γ_{I} is computed from the correspondent adjacent variables. This discretization leads to sparse matrices $\mathbb{M}$ and $\mathbb{K}$ of size $27,996 \times 27,996$, $\mathbb{H}$ of size $21,894 \times 21,894$ and $\mathbb{V}$ of size $21,894 \times 43,026$. Even if the BEM matrix $\mathbb{H}$ is not sparse, due to the presence of many trivial entries it is stored in the compressed sparse `Matlab` column format, that allows to reduce the amount of memory by almost 20%. On the other side, the matrix $\mathbb{V}$ is stored in full or $\mathcal{H}$-matrix format.
In the following, we will numerical evaluate the quality factor Q related to the excitation of the resonator in its axial and bending modes. In particular the axial mode indicates a cantilever stretching along its principal axis, while the bending mode describes a cantilever flexion, as shown in Figures 2 and 3 respectively.

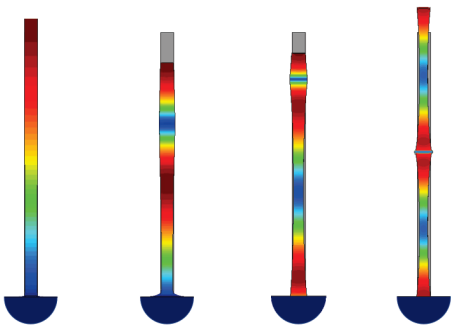

Figura 2: Test problem. From the left to the right, cantilever beam excited in its first, second third and fourth axial modes.

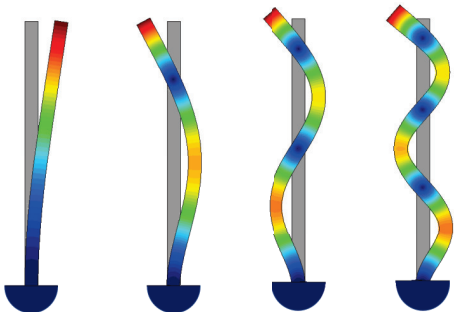

Figura 3: Test problem. From the left to the right, cantilever beam excited in its first, second third and fourth bending modes.

4.2. Cantilever beam excited in its axial modes

If the resonator is excited in its n-th axial mode, an analytical estimate for the quality factor is provided in [7], i.e.

$$Q = \frac{2}{2n-1}\,\frac{0.88}{\pi}\,\frac{L^2}{VH}\,, \quad n = 1, 2, ... \tag{19}$$

On the other side, the theoretical eigenfrequency for a clamped cantilever beam is given by the formula [1]:

$$\widetilde{\omega} = \frac{(2n-1)\,\pi}{2L}\sqrt{\frac{E}{\varrho}}\,. \tag{20}$$

Linear system (13) is solved using a GMRES solver with tolerance $\varepsilon_{\text{GMRES}} = 10^{-4}$ and it needs only $N_{\text{GMRES}} = 10$ iterations to reach convergence. In Table 1 we show, for $n = 1, ..., 4$, the analytical estimates and the obtained numerical values of $\widetilde{\omega}$ and Q.
Let us observe that, using the above described FEM mesh, the maximum relative error obtained on the eigenfrequencies is 3.6%; for this reason, we did not refine it anymore. The relative gap between numerical and analytical quality factor is a little bit higher, but reasonable, for the meshsizes adopted. Further, remembering formulas (1) and (16), we observe that a relative variation δ on $\widetilde{\omega}$ implies an expected at least $2\,\delta$ relative variation on Q w.r.t. the analytical estimate. Nevertheless, for growing frequencies the influence of the additional hemisphere, w.r.t. the analytical procedure, becomes greater, making the proposed approach more reliable than the analytical one.

n	numerical Q	analytical Q	numerical $\widetilde{\omega}$ ($^{\text{rad}}/_{\text{s}}$)	analytical $\widetilde{\omega}$ ($^{\text{rad}}/_{\text{s}}$)
1	127.12	112.05	1,286,000,000	1,310,000,000
2	34.82	37.35	3,819,000,000	3,930,000,000
3	16.76	22.41	6,347,000,000	6,550,000,000
4	13.80	16.01	8,844,000,000	9,170,000,000

Tabella 1: Numerical results for axial modes and related analytical estimates.

In Figure 4, 5, 6, 7, the *magnitude* of the three components of the displacement field computed on the surface $\partial\Omega_{\text{B}}$, respectively for the first, second, third and fourth considered axial modes, are depicted. As on can observe, in all cases, no spurious reflections can be noticed along the circular truncation line on the substrate and a perfectly symmetric behavior of the solution can be appreciated. Further, towards the truncation of the substrate the displacement is vanishing.

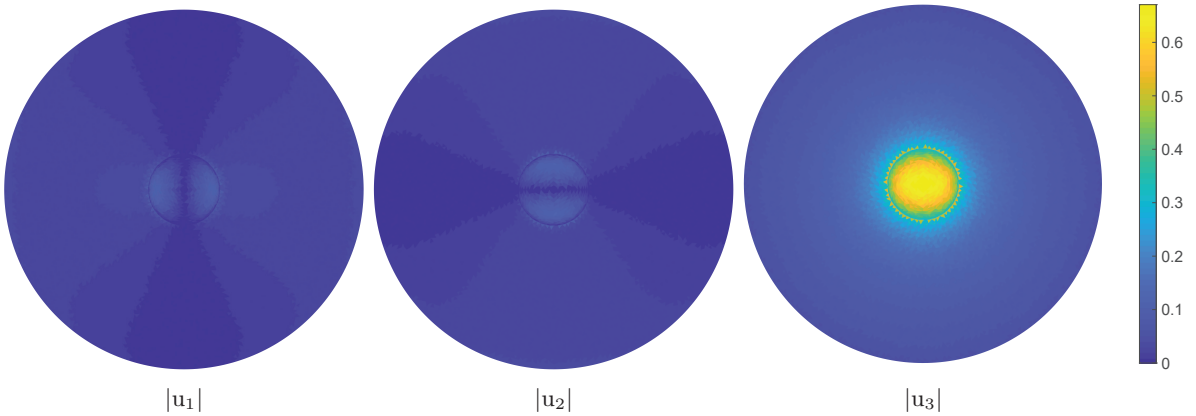

Figura 4: Resonator excited in its first axial mode. Top view of the *magnitude* of the components of the computed displacement field on the surface $\partial\Omega_{\mathrm{B}}$.

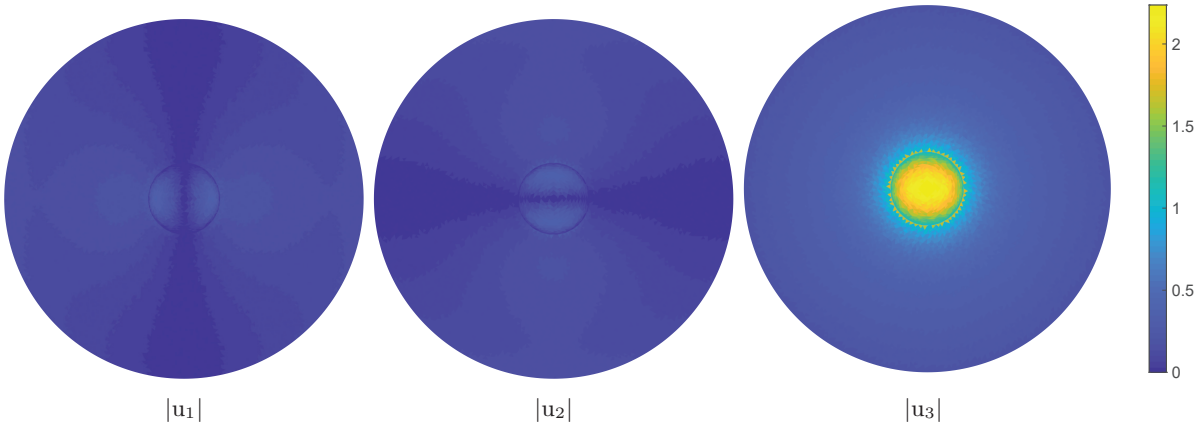

Figura 5: Resonator excited in its second axial mode. Top view of the *magnitude* of the components of the computed displacement field on the surface $\partial\Omega_{\mathrm{B}}$.

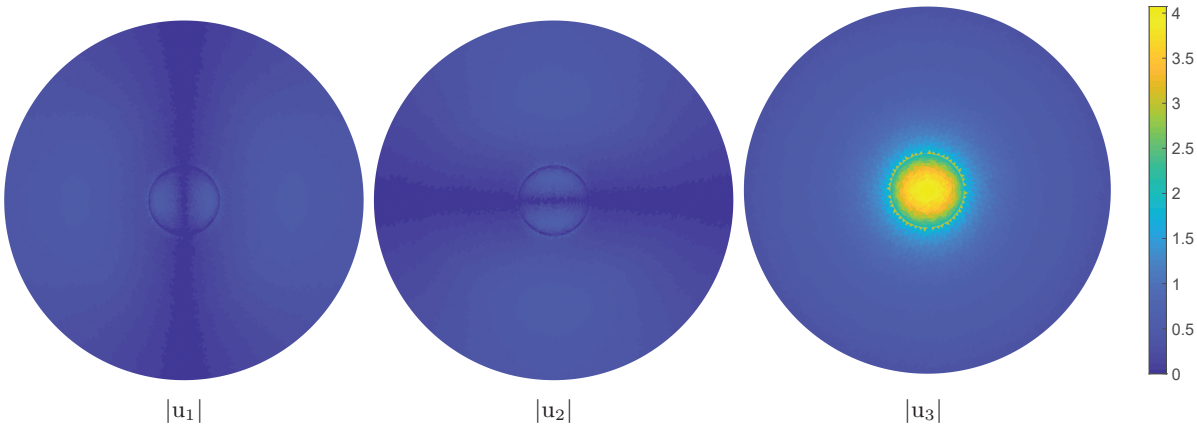

Figura 6: Resonator excited in its third axial mode. Top view of the *magnitude* of the components of the computed displacement field on the surface $\partial\Omega_{\mathrm{B}}$.

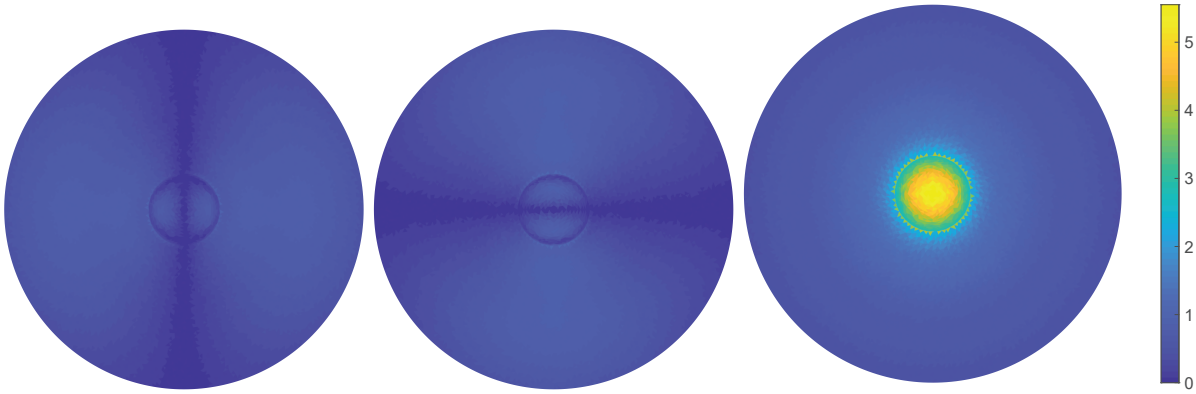

Figura 7: Resonator excited in its fourth axial mode. Top view of the *magnitude* of the components of the computed displacement field on the surface $\partial\Omega_B$.

4.3. Cantilever beam excited its bending modes

If the resonator is excited in its n-th bending mode, the following analytical estimate for the quality factor is reported in [7]:

$$Q = \frac{3.9}{c_n} \frac{3^4}{(2\,k_n\,L)^4} \frac{L^5}{V\,H^4}\,, \quad n = 1, 2, ... \tag{21}$$

where $c_n = \left[tanh^2(\frac{k_n L}{2})\right]^{(-1)^{n-1}}$ with $k_n\,L\,, n = 1, 2, ...$ the positive solutions of the nonlinear equation

$$\cos(k_n\,L)\,\cosh(k_n\,L) + 1 = 0\,; \tag{22}$$

on the other side, the theoretical eigenfrequency of a perfectly clamped cantilever beam is given by the formula [1]:

$$\widetilde{\omega} = (k_n\,L)^2 \frac{H}{L^2} \sqrt{\frac{E}{12\,\rho}}\,. \tag{23}$$

Linear system (13) is solved using a GMRES solver with tolerance $\varepsilon_{\text{GMRES}} = 10^{-4}$ and it needs only $N_{\text{GMRES}} = 10$ iterations to reach convergence. In Table 2 we show, for $n = 1, ..., 4$, the analytical estimates and the numerical values of $\widetilde{\omega}$ and Q. As one can see, here the maximum relative error obtained on the eigenfrequencies is 7.2% and the obtained results on quality factors are strictly adherent to analytical predictions (maximum relative gap 8%), except for the Q value of the first bending mode, whose order of magnitude is $O(10^6)$. In this scenario, algorithmic errors could affect any numerical method, but it's worth noting that huge quality factors have little engineering significance, since in this case dissipative phenomena other than anchor losses usually dominate.

n	$k_n\,L$	numerical Q	analytical Q	numerical $\widetilde{\omega}$ ($^{\text{rad}}/_{\text{s}}$)	analytical $\widetilde{\omega}$ ($^{\text{rad}}/_{\text{s}}$)
1	1.875	6,723,495	4,743,160	41,910,000	42,320,000
2	4.694	64,919	62,731	255,930,000	265,250,000
3	7.855	8,631	8,311	704,880,000	742,790,000
4	10.996	2,335	2,161	1,349,790,000	1,455,610,000

Tabella 2: Numerical results for bending modes and related analytical estimates.

In Figure 8, 9, 10, 11, the *magnitude* of the three components of the displacement field computed on the surface $\partial\Omega_B$, respectively for the first, second, third and fourth considered bending modes,

are depicted. As already observed in axial modes simulations, no spurious reflections appear along the circular truncation line on the substrate and a perfectly symmetric behavior of the solution can be appreciated. Further, towards the truncation of the substrate the displacement is vanishing.

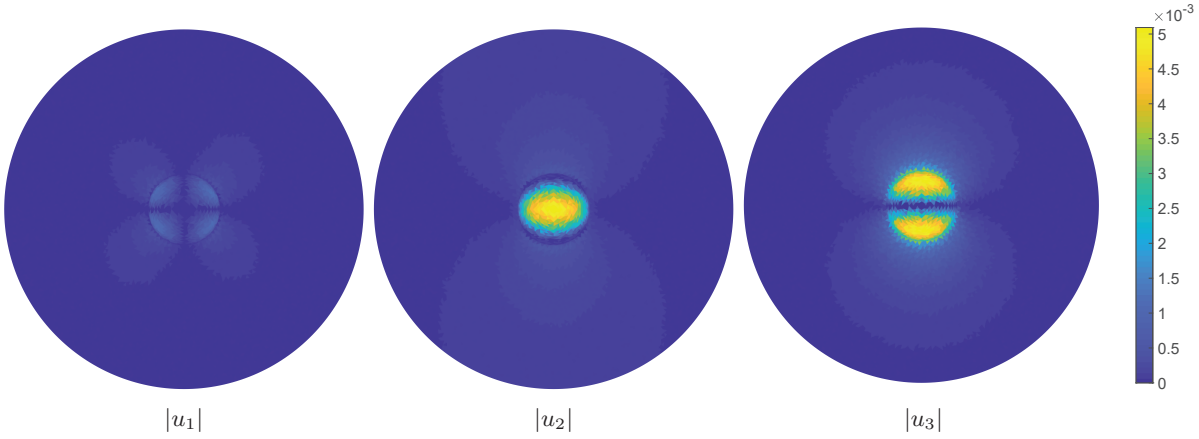

Figura 8: Resonator excited in its first bending mode. Top view of the *magnitude* of the components of the computed displacement field on the surface $\partial\Omega_{\mathrm{B}}$.

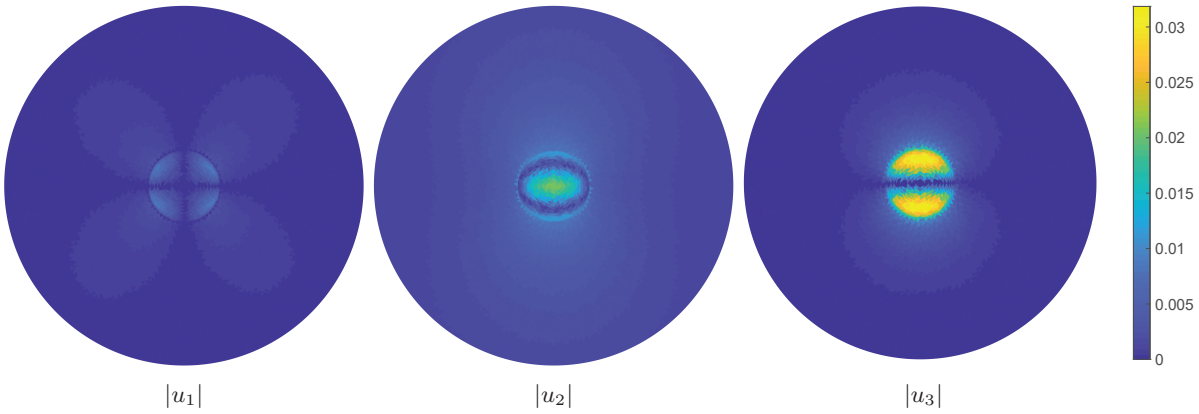

Figura 9: Resonator excited in its second bending mode. Top view of the *magnitude* of the components of the computed displacement field on the surface $\partial\Omega_{\mathrm{B}}$.

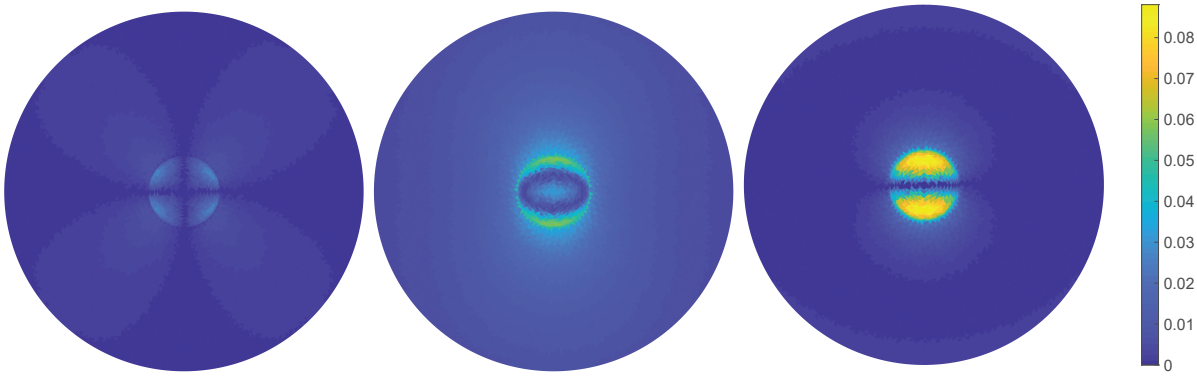

$|u_1|$ $|u_2|$ $|u_3|$

Figura 10: Resonator excited in its third bending mode. Top view of the *magnitude* of the components of the computed displacement field on the surface $\partial\Omega_{\mathrm{B}}$.

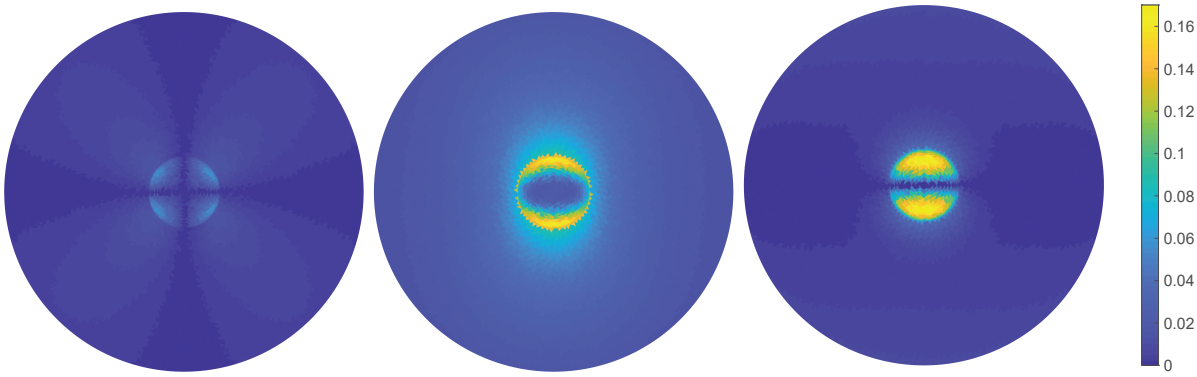

$|u_1|$ $|u_2|$ $|u_3|$

Figura 11: Resonator excited in its fourth bending mode. Top view of the *magnitude* of the components of the computed displacement field on the surface $\partial\Omega_{\mathrm{B}}$.

4.4. $\mathcal{H}$-matrix based memory saving and acceleration

To assemble the hierarchical representation $\mathbb{V}_{\mathcal{H}}$ of the matrix $\mathbb{V}$, a hierarchical cluster tree is constructed with a minimum number of elements $n_{\mathrm{LEAF}} = 100$, resulting in 31 clusters and 10 cluster levels. The parameter $\eta = 3$ is used in the admissibility condition (15) with, consequently, 894 full-rank and 1,468 low-rank block clusters in the block cluster tree. In Figure 12, on the left, we give an illustration of the block repartition in the $\mathcal{H}$-matrix $\mathbb{V}_{\mathcal{H}}$, that does not depend on the angular frequency $\widetilde{\omega}$ and consequently is the same for all the considered modes, in order to better point out how the choice of η leads to large low-rank blocks (light/ cyan blocks) and small full blocks (dark/ pink blocks). Since this structure depends on the mesh of BEM domain, in Figure 12, on the right, we show the triangulation of $\partial\Omega_{\mathrm{B}}$. The threshold $\varepsilon_{\mathrm{ACA}} = 10^{-4}$ is used in the ACA algorithm to compute the low-rank approximations. This last parameter is responsible of the memory saving.

To test the accuracy of our method when the $\mathcal{H}$-matrix representation of the matrix $\mathbb{V}$ is used to accelerate the coupling, we introduce the relative error

$$E_{Q,\mathcal{H}} := \frac{|Q - Q_{\mathcal{H}}|}{|Q|}, \tag{24}$$

associated to the approximate quality factor $Q_{\mathcal{H}}$, with respect to the the quality factor Q evaluated with the standard BEM-FEM coupling. In Table 3, we report these quantities for the four axial and

the four bending modes considered in the previous sections. Additionally, we focus our attention on the percentage of the memory saving, defined as

$$m_s(\%) := 100 \cdot \left(1 - \frac{\text{storage}(\mathbb{V}_{\mathcal{H}})}{\text{storage}(\mathbb{V})}\right). \tag{25}$$

As we expected, we observe an error lower than 10^{-3}; this is not surprising since, as we have already remarked, ε_{ACA} gives us an a priori estimate on the precision of the $\mathcal{H}$-matrix/vector product. In Table 3, it is also visible the high memory saving obtained with the $\mathcal{H}$-matrix compression technique. We remark that approximately only the 10% of the entries of the original matrix $\mathbb{V}$ (of size 21,894×43,026) is needed in its $\mathcal{H}$-matrix representation.

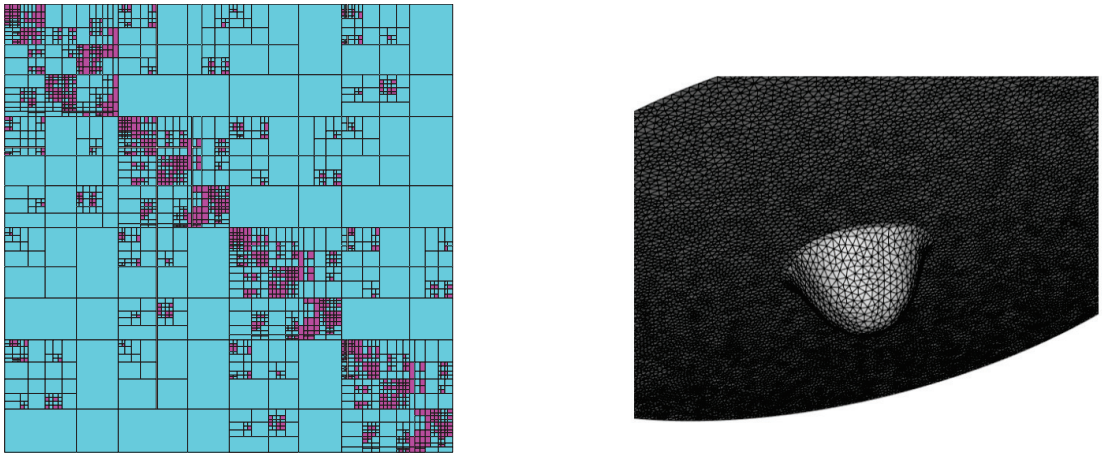

Figura 12: Resonator excited in its first four axial or bending modes. $\mathcal{H}$-matrix representation of the matrix $\mathbb{V}$ (left), corresponding to the mesh of the BEM subdomain (right). The light/ cyan blocks are stored as low-rank matrices, while the dark/ pink blocks are stored as full matrices.

	n	$E_{Q,\mathcal{H}}$	m_s
axial	1	$1.91E-07$	89%
	2	$1.36E-06$	89%
	3	$1.14E-08$	88%
	4	$9.24E-07$	88%
bending	1	$3.93E-04$	89%
	2	$2.46E-05$	89%
	3	$1.51E-06$	89%
	4	$1.34E-05$	89%

Tabella 3: Resonator excited in its first four axial and bending modes. Errors and memory saving for the acceleration of the computation in the BEM subdomain, with the $\mathcal{H}$-matrix approximation of the matrix $\mathbb{V}$.

Remark 3. Recalling that elapsed time measurements are code-, software- and computer-dependent and that the FEM part of the algorithm has been implemented in Fortran language, while the BEM part of the algorithm has been implemented in `Matlab`, we report here results for the first axial mode simulation (the other cases are similar). The FEM computation is performed in few seconds, from $t_{\text{F}} \simeq 1.0\,\text{s}$ to $t_{\text{F}} \simeq 5.0\,\text{s}$ according to the platform. The BEM computation, run on a Windows10 HP Z620 Workstation with two Intel(R) Xeon(R) CPU E5-2620 0 processors, 32Gbytes of RAM, requires $t_{\text{B}} \simeq 11.6\,\text{s}$. This last value is reduced to $t_{\text{B},\mathcal{H}} \simeq 9.6\,\text{s}$, with an elapsed time saving of nearly 20%, when we use the $\mathcal{H}$-matrix approach for the generation of the RHS of

the BEM linear system. Hence, BEM turns out to be really competitive with FEM. Let us remark that the reported BEM results have been evaluated calling the most robust `Matlab` function in use, which is based on multiple calls and takes the median of all measurements, and they are in perfect agreement with the results in [13], where a deep investigation of the performances of the complexity in terms of CPU time of $\mathcal{H}$-matrix based iterative solvers has been presented for 3D frequency-domain elastodynamic problems. Summarizing, we can assert that the proposed procedure has an overall negligible time cost.

5. Conclusions

The spread of MEMS in the consumer world recently triggered a revolution of user interfaces in gaming, mobile phones and navigation. Similarly, in the near future, new generations of sensors and actuators will dramatically impact our lives and will enable the evolution of Internet of Things in its different declinations such as Smart City, Home, Farming, Objects and Driving. These innovative MEMS come with a cost, i.e. an increase of the device complexity. Outstanding performances demand a novel systematic approach for the design of multiphysics MEMS. The description of the dynamical behavior of MEMS devices like gyroscopes, micromirrors, loudspeakers and energy harvesters generates time-dependent, nonlinear, multi-physics models including electromagnetics, piezoelectricity, fluid-structure interaction. Problems are set on intricate geometrical configurations and burdened by uncertainties on material parameters and fabrication imperfections. This makes traditional full-order simulation strategies extremely expensive, if not infeasible. In particular an agile a priori estimation of dissipation is of paramount importance in order to mitigate power consumption. Anchor losses have been clearly identified as one of the main sources of dissipation in main MEMS families like resonators. Costly simulation strategies have been proposed in the literature, but research is still active in the field.
In this paper, we have presented a fast one-shot BEM-FEM approach for estimating anchor losses in MEMS. This method turns out to give reliable evaluations of the quality factor of the resonator, that gives us information about the performances of the device, as long as other dissipative phenomena other than anchor losses dominate. In order to reduce as much as possible the elapsed computational time in the BEM subdomain, we have studied the structure of the matrices involved and we have used the fast $\mathcal{H}$-matrix/vector product, that allows to accelerate the computation of the RHS of the BEM linear system. We have compared and discussed the Q values obtained by the proposed approach w.r.t. analytical predictions, based on physical model simplifications, provided in literature for the configuration of a cantilever beam resting on a semi-infinite space, excited in its both axial and bending modes. The accuracy of the method and the small observed elapsed times will allow the analysis of real-life MEMS resonators, as above recalled, which will be targeted in future investigations.

Acknowledgements. The Authors are in debt with Professor M. Diligenti, for fruitful discussions and illuminating advices, and are grateful to the anonymous Associate Editor and Reviewers for their stimulating comments.
This research benefits from the HPC (High Performance Computing) facility of the University of Parma, Italy.

Funding. First and second Authors were partially supported by Italian GNCS-INdAM 2020 research program *"Metodologie innovative per problemi di propagazione di onde in domini illimitati: aspetti teorici e computazionali"*.

References

[1] A. Frangi, A. Bugada, M. Martello, P.T. Savadkoohi, Validation of PML-based models for the evaluation of anchor dissipation in MEMS resonators, European J. Mech. A/Solids 37 (2013) 256–265.

[2] Z. Hao, Vibration displacement on substrate due to the time-harmonic stress source from a micromechanical resonator, Journal of Sound and Vibration 322 (2009) 196–215.

[3] Y. Jimbo, K. Itao, Energy loss of a cantilever vibrator, Journal of the Horological Institute of Japan 47 (1968) 1-15.

[4] M.C. Cross, R. Lifshirz, Elastic wave transmission at an abrupt junction in a thin plate with application to heat transport and vibrations in mesoscopic system, Physical Review B 64 (2001) 085324–1–22.

[5] J.A. Judge, D.M. Photiadis, J.F. Vignola, B.H. Houston, J. Jarzynski, Attachment losses of micromechanical and nanomechanical resonators in the limits of thick and thin support structures, Journal of Applied Physics 101 (2007) 013521.

[6] G.D. Cole, I. Wilson-Rae, K. Werbach, M.R. Vanner, M. Aspelmeyer, Phonon tunnelling dissipation in mechanical resonators, Nature Communication 2 231 (2011) 1-8.

[7] I. Wilson-Rae, Intrinsic dissipation in nanomechanical resonators due to phonon tunnelling, Physical Review B 77 (2008) 245–418.

[8] R. Ardito, C. Comi, A. Corigliano, A. Frangi, Solid damping in micro electro mechanical systems, Meccanica 43 (2008) 419-428.

[9] J. Choi, M. Cho, J. Rhim, Efficient prediction of the quality factors of micromechanical resonators, Journal of Sound and Vibration 329 (2010) 84-95.

[10] A. Aimi, M. Diligenti, A. Frangi, C. Guardasoni, Neumann exterior wave propagation problems: computational aspects of 3D energetic Galerkin BEM, Computational Mechanics 51 (4) (2013) 475-493.

[11] S. Falletta, G. Monegato, L. Scuderi, On the discretization and application of two space-time boundary integral equations for 3D wave propagation problems in unbounded domains, Applied Numerical Mathematics 124 (2018) 22–43.

[12] L. Desiderio, S. Falletta Efficient Solution of Two-Dimensional Wave Propagation Problems by CQ-Wavelet BEM: Algorithm and Applications, SIAM Journal on Scientific Computing 42 (4) (2020) B894-B920.

[13] L. Desiderio, $\mathcal{H}$-matrix based solvers for 3D elastodynamic Boundary Integral Equations, PhD Thesis Paris-Saclay University (2017).

[14] L. Desiderio, An $\mathcal{H}$-matrix based direct solver for the boundary element method in 3D elastodynamics, AIP Conference Proceedings 1978 (2018) 120005.

[15] Z. Fu, W. Chen, P. Wen, C. Zhang, Singular boundary method for wave propagation analysis in periodic structures, Journal of Sounds and Vibration 425 (2018) 170–188.

[16] W. Li, A fast singular boundary method for 3D Helmholtz equation, Computer and Mathematics with Applications 77 (2019) 525–535.

[17] J. Li, Z. Fu, W. Chen, Q.-H. Qin, A regularized approach evaluating originintensity factor of singular boundary method for Helmholtz equation with high wavenumbers, Engineering Analysis with Boundary Elements 101 (2019) 165–172.

[18] T. Ruberg, M. Schanz, Coupling finite and boundary element methods for static and dynamic elastic problems with non-conforming interfaces, Comput. Methods Appl. Mech. Engrg. 198 (2008) 449–458.

[19] A. Aimi, M. Diligenti, A. Frangi, C. Guardasoni, Energetic BEM-FEM coupling for wave propagation in 3D multidomains, International Journal for Numerical Methods in Engineering 97 (2014) 377-394.

[20] S.M. Kirkup, S. Amini, Solution of the Helmholtz eigenvalue problem via the Boundary Element Method, International Journal for Numerical Methods in Engineering 36 (1993) 321-330.

[21] k. Matsushima, H. Isakari, T. Takahashi, T. Matsumoto, An investigation of eigenfrequencies of boundary integral equations and the burton-Miller formulation in two-dimensional elastodynamics, Int. J. Comp. Meth. and Exp. Meas. 101 (6) (2018) 1127-1137.

[22] J. Dominguez, Dynamic Stiffness of Rectangular Foundations, Soils publication, Massachusetts Institute of Technology, Department of Civil Engineering, Constructed Facilities Division, (1978).

[23] T.J.R. Hughes, The Finite Element Method: Linear Static and Dynamic Finite Element Analysis, Dover Civil and Mechanical Engineering, Dover Publications, (2000).

[24] R.B. Lehoucq, D.C. Sorensen, Deflation techniques for an implicitly restarted Arnoldi iterations, SIAM J. Matrix Analysis and Applications 17 (4) (1996) 789–821.

[25] M. Guiggiani, A. Gigante, A general algorithm for multidimensional Cauchy principal value integrals in the boundary element method, Journal of Applied Mechanics 57 (1990) 906–915.

[26] Y. Saad, M.H. Schultz, GMRES: a generalized minimal residual algorithm for solving nonsymmetric linear system, SIAM Journal on Scientific Computing 7 (1986) 856–869.

[27] W. Hackbusch, A sparse arithmetic based on $\mathcal{H}$-Matrices. Part I: Introduction to $\mathcal{H}$-Matrices, Computing 62 (1999) 89–108.

[28] M. Bebendorf, S. Rjasanow, Adaptive low-rank approximation of collocation matrices, Computing 70 (2003) 1–24.

[29] S. Rjasanow, L. Weggler Matrix valued adaptive cross approximation, Mathematical Methods in the Applied Sciences 40 (7) (2016) 2522–2531.

[30] A.M. Haider, M. Schanz, Adaptive Cross Approximation for BEM in Elasticity, Journal of Theoretical and Computational Acoustics 27 (1) (2019).

[31] S. Chaillat, L. Desiderio, P. Ciarlet Jr, *Theory and implementation of $\mathcal{H}$-matrix based iterative and direct solvers for Helmholtz and elastodynamic oscillatory kernels*, Journal of Computational Physics, **351**, (2017), 165–186.

[32] D.M. Photiadis, J.A. Judge, Attachment losses of high Q oscillators, Applied Physics Letters 85(2004) 482–484.

[33] R.B. Lehoucq, D.C. Sorensen, C. Yang, ARPACK, Users' Guide: Solution of large scale eigenvalue problems with implicitly restarted Arnoldi methods, `http://www.caam.rice.edu/software/ARPACK`, (1997).

[34] O. Schenk, K. Gartner, PARDISO, User Guide Version 4.1.2, `http://www.pardiso-project.org`, (2011).

[35] J. Dominguez, Boundary elements in dynamics, Wit Press, (1993).